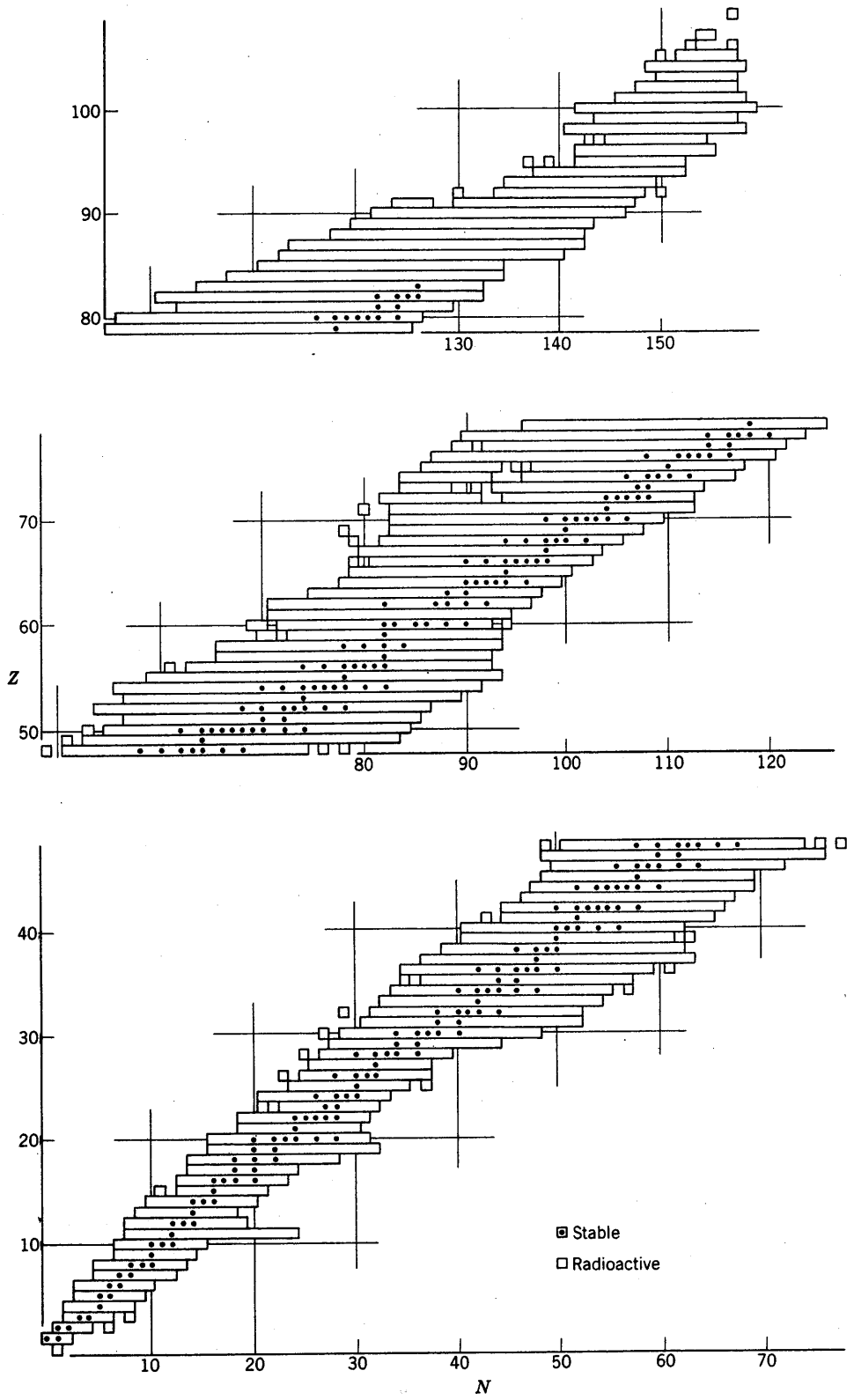
100
90
80
130
140
150
70
60
Z
50
80
90
100
110
120
40
30
20
10
Stable
Radioactive
10
20
30
40
50
60
70
N

Figure 14-5
Stable and radioactive isobars at low mass number. Isotopic abundances are quoted for the stable nuclides, and radioactive half-lives are given for the unstable isobars.

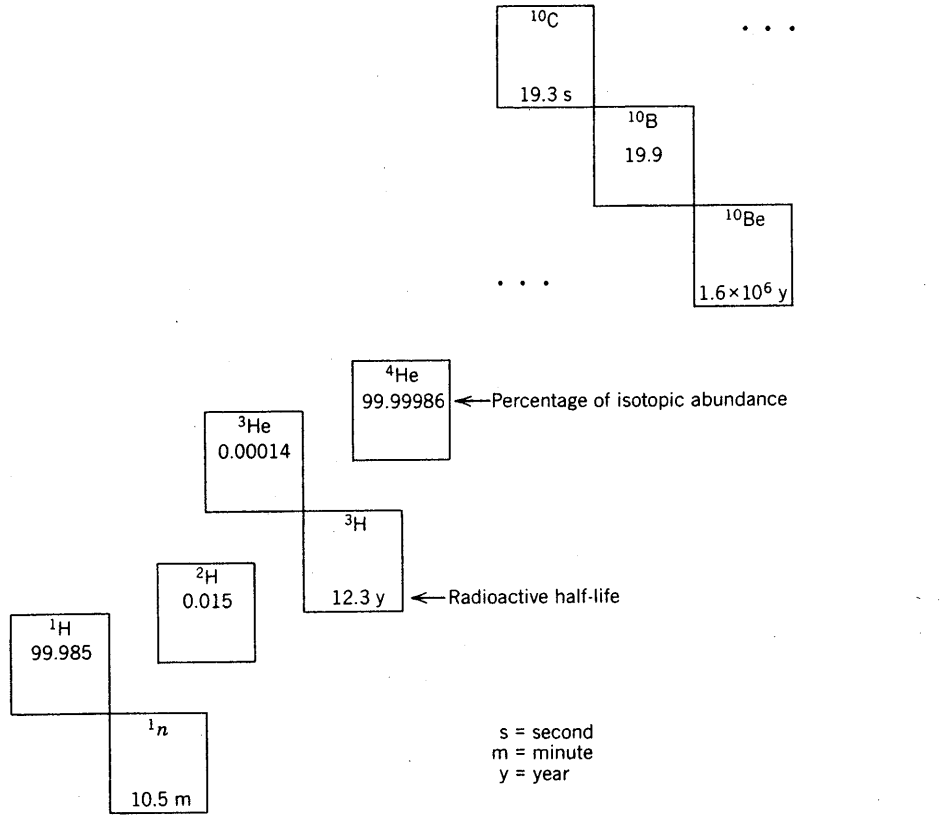

mass numbers as qualitative indications of the unusual stability of the $A = 4$ nuclide ^{4}He. The two gaps tell us that it is not favorable to add one more nucleon to the $A = 4$ system or to bind two such systems together.

We learn several interesting lessons just by counting the nuclides according to the following four possible combinations of proton and neutron numbers. Of the 268 existing stable nuclei (including those that are extremely long-lived), there are

	159 with even Z and even N	(even–even),	even A
	53 with even Z and odd N	(even–odd),	odd A
	50 with odd Z and even N	(odd–even),	odd A
and	6 with odd Z and odd N	(odd–odd).	even A

The stable odd-A nuclei exist in roughly equal numbers of even–odd and odd–even varieties. This observation is a hint that the nuclear force does not distinguish between protons and neutrons. The distribution of the stable even-A nuclei is more remarkable

Figure 14-6
Schematic plan of Hofstadter's electron-scattering experiment.

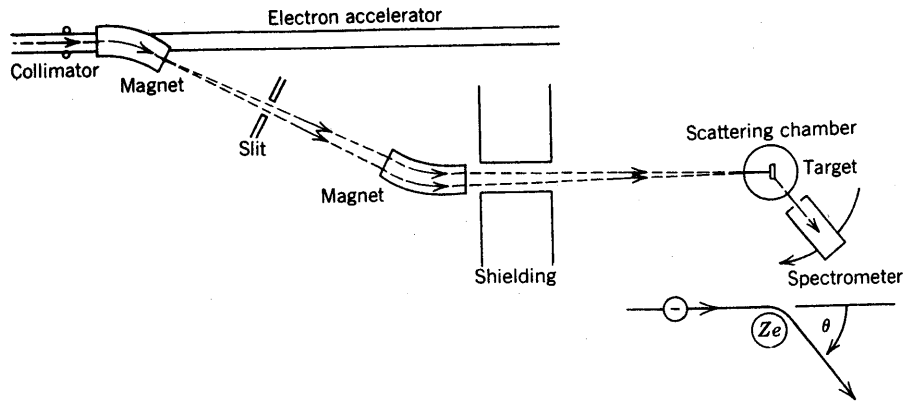

experiments in which electrons are scattered by the nucleus. These data can be used to determine the nuclear radius.

The electron-scattering experiments had to wait for the construction of high-energy electron accelerators. A comprehensive series of investigations of nuclei was finally undertaken by R. Hofstadter and his associates in 1953. Eventually, these studies were extended to include measurements of the internal electromagnetic structure of the proton and the neutron. Thus, the whole range of electron-scattering experiments gave a description of the constituents of the nucleus as well as the nucleus itself.

Figure 14-6 shows a sketch describing Hofstadter's means of observation of the elastic-scattering process

$$e + \mathrm{X} \rightarrow e + \mathrm{X}.$$

The equipment includes an electron accelerator and deflecting magnets to prepare the high-energy electron beam, a scattering target of species X, and a spectrometer to detect electrons scattered elastically in directions given by the indicated scattering angle θ. This apparatus constitutes an elaborate high-energy device for the study of electron diffraction, since the angular distribution of the scattered electrons has the appearance of a diffraction pattern. We represent these observations by means of the differential cross section $d\sigma/d\Omega$ for elastic electron scattering, an angle-dependent quantity analogous to the Rutherford cross section for the scattering of α particles. Experimental values of $d\sigma/d\Omega$ are plotted in Figure 14-7 for a single beam energy and for several nuclear targets. We see the characteristic features of a diffraction pattern in each of the graphs, as the cross sections fall rapidly from the forward direction at $\theta = 0$ and exhibit small peaks at other angles.

The behavior of $d\sigma/d\Omega$ is similar to the diffraction of light by a spherical obstacle with a dense interior and a diffuse surface. A good characterization of electron scattering can be given in these terms by adopting a spherical model of the nucleus in which the nuclear charge density has the form

$$\rho(r) = \frac{\rho_1}{1 + e^{(r-R)/z_1}}. \qquad (14\text{-}2)$$

Figure 14-7
Differential cross sections for elastic electron scattering at 183 MeV. Data are plotted versus scattering angle θ for calcium, indium, and gold targets.

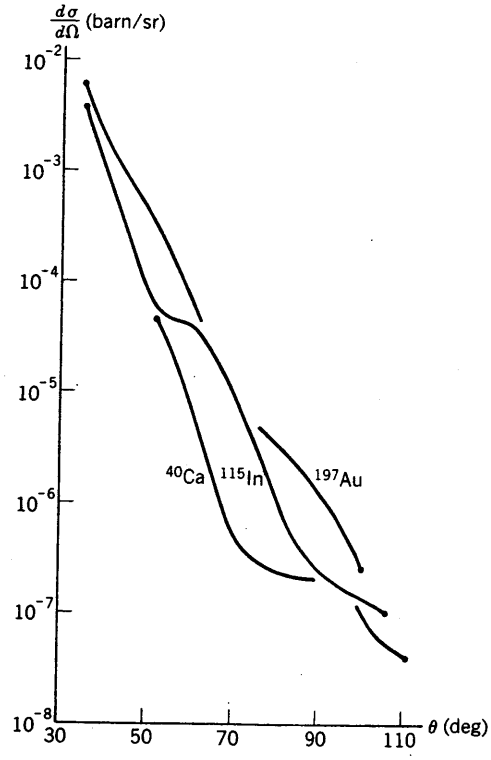

This expression is like a Fermi distribution in which the two parameters R and z_1 control the r dependence. The coefficient ρ_1 is proportional to the central charge density

$$\rho(0) = \frac{\rho_1}{1 + e^{-R/z_1}},$$

so that ρ_1 and $\rho(0)$ are approximately equal for $R \gg z_1$. We can interpret the significance of these features with the aid of Figure 14-8. The illustrated charge density falls through the value $\rho_1/2$ at $r = R$, dropping from 90% to 10% of the maximum density over a small distance given by the indicated surface thickness t. The latter quantity is directly related to the parameter z_1 in Equation (14-2). We leave the derivation of this relation to Problem 3 at the end of the chapter.

The treatment of electron-scattering data for different beam energies and various nuclei leads to the deduction of charge densities like the ones shown in Figure 14-9. We select these particular results to correspond to the cross sections plotted in Figure 14-7. The graphs indicate a decrease of the central charge density $\rho(0)$ and an increase of the radius parameter R as nuclei of increasing nucleon number are considered, while the surface thickness remains essentially unchanged. This analysis determines a nuclear radius R that grows with mass number A according to the

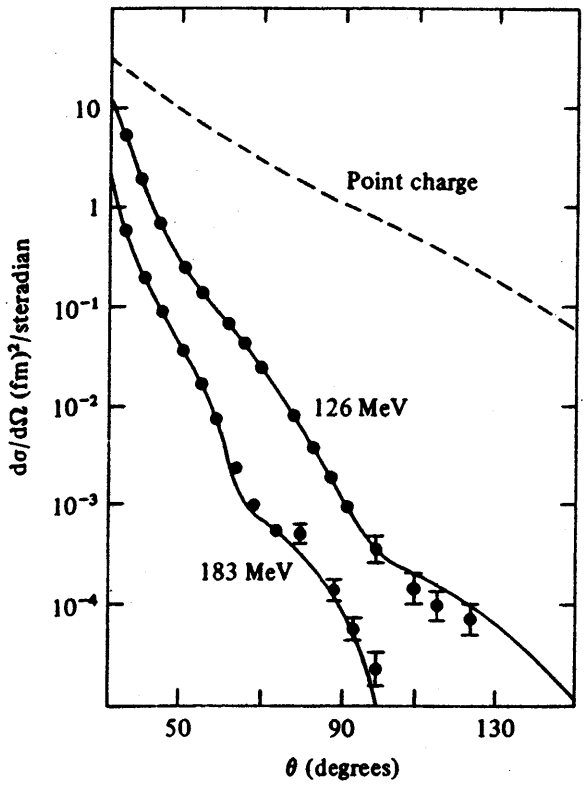

Fig. 4.1 Experimental elastic electron-scattering differential cross-section from gold $^{197}_{79}$Au at energies of 126 MeV and 183 MeV. The fitted curves are calculated with an assumed charge distribution of the form given by equation (4.1), with $R = 6.63$ fm, $a = 0.45$ fm. The cross-section to be expected, at 126 MeV, if the gold nucleus had a point charge is shown for comparison. (Data and theoretical curves taken from Hofstadter, R. (1963), *Electron Scattering and Nuclear and Nucleon Structure*, New York: Benjamin.)

$$\rho_{ch}(r) = \frac{\rho_{ch}^0}{1 + e^{(r-R)/a}}, \tag{4.1}$$

where the parameters to be determined are R and a, and ρ_{ch}^0 is a normalisation constant chosen so that

$$\int \rho_{ch}(r) d^3\mathbf{r} = 4\pi \int_0^\infty \rho_{ch}(r) r^2 dr = Z.$$

It should be stressed that the choice of this expression has no fundamental significance, it just conveniently describes a charge distribution which extends almost uniformly from the centre of the nucleus to a distance R, and falls to zero over a well-defined surface region of thickness $\sim a$. This picture is consistent with the results of direct inversion.

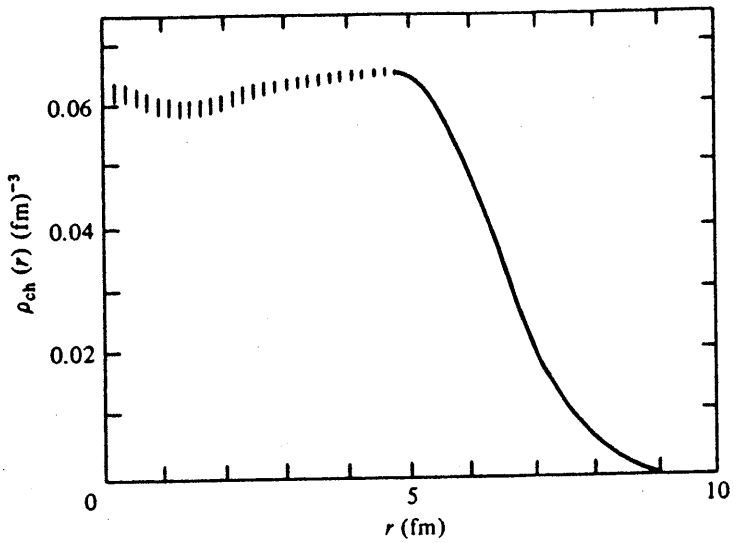

Fig. 4.2 The electric charge density of $^{208}_{82}$Pb from a model-independent analysis of electron scattering data. The bars indicate the uncertainty. (Friar, J. L. & Negele, J. W. (1973), *Nucl. Phys.* **A212**, 93.)

In Fig. 4.3 we show nuclear charge distributions for a light ($^{16}_{8}$O), a medium ($^{109}_{47}$Ag) and a heavy ($^{208}_{82}$Pb) nucleus obtained from experimental scattering data, using this parametrisation of the charge density. The corresponding values of R and a are given in Table 4.1.

As the examples in the table indicate, it appears that there is a well-defined 'surface region' which has much the same width for all nuclei, even light ones.

4.2 Muon interactions

The negative muon is another leptonic probe of nuclear charge. Its properties, other than its mass of $m_\mu \approx 207\, m_e$ and its mean life of

Table 4.1. *Nuclear radii (R) and nuclear surface widths (a)*

Nucleus	R (fm)	a (fm)	$R/A^{\frac{1}{3}}$ (fm)
$^{16}_{8}$O	2.61	0.513	1.04
$^{109}_{47}$Ag	5.33	0.523	1.12
$^{208}_{82}$Pb	6.65	0.526	1.12

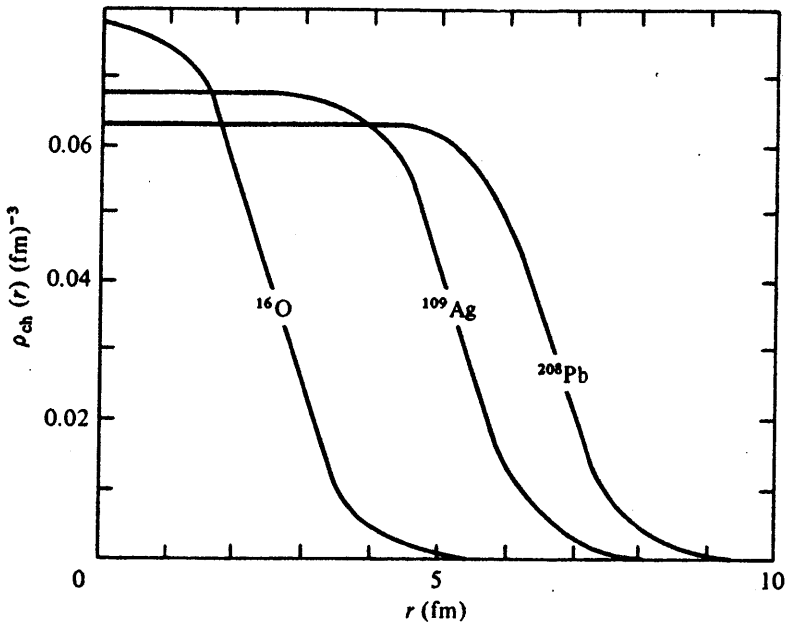

Fig. 4.3 The electric charge density of three nuclei as fitted by $\rho_{ch}(r) = \rho^0_{ch}/[1 + \exp((r - R)/a)]$. The parameters are taken from the compilation in Barrett, R. C. & Jackson, D. F. (1977), *Nuclear Sizes and Structure*, Oxford: Clarendon Press.

2.2×10^{-6} s, are similar to those of the electron. However, the radius of its lowest Bohr orbit in an atom of charge Z is $(4\pi\varepsilon_0)\hbar^2/m_\mu Ze^2$, and this is smaller than the corresponding electron orbit by a factor (m_e/m_μ). For $Z = 50$ the radius is only 5 fm. Hence the wave-functions of the lowest muonic states will lie to a considerable extent within the distribution of nuclear charge, particularly in heavy nuclei, and the energies of these states will therefore depend on the details of the nuclear charge distribution.

Experimentally, negative muons are produced in the target material by the decay of a beam of negative pions, and are eventually captured in outer atomic orbitals. Before they decay, many muons fall into lower orbits, emitting X-rays in the transitions. The measured energies of these X-rays may be compared with those calculated with various choices of parameters for $\rho_{ch}(r)$. Values of R and a, found in this way, agree well with results from electron scattering.

4.3 The distribution of nuclear matter in nuclei

From the distribution of charge in a nucleus, which as we have seen can be determined by experiment, we can form some idea of the distribution

of nuclear matter. If the proton were a point object, we could identify the proton number density $\rho_p(r)$ with $\rho_{ch}(r)$. Since the strong nuclear forces which bind nucleons together are charge independent and of short range, we can assume that to a good approximation the ratio of neutron density ρ_n to proton density ρ_p is the same at all points in a nucleus, i.e. $\rho_n(r)/\rho_p(r) = N/Z$. Then the total density of nucleons $\rho = \rho_n + \rho_p$ can be expressed as $\rho = (A/Z)\rho_{ch}$, where $A = N + Z$. The resulting nuclear matter densities for the same nuclei we took in Fig. 4.3 are plotted in Fig. 4.4. These densities are only approximate, since we have neglected the finite size of both proton and neutron and the effect of Coulomb forces, but they indicate that at the centre of a nucleus the nuclear matter density ρ is roughly the same for all nuclei. It increases with A, but appears to tend to a limiting value ρ_0 of about 0.17 nucleons fm^{-3} for large A. The existence of this limiting value ρ_0, known as the 'density of nuclear matter', is an important result. Consistently with this, we find (Table 4.1), that the 'radius' R of a nucleus is very closely proportional to $A^{\frac{1}{3}}$, and, approximately, $(4\pi/3)R^3\rho_0 = A$. We shall take

$$\rho_0 = 0.17 \text{ nucleons fm}^{-3} \tag{4.2}$$

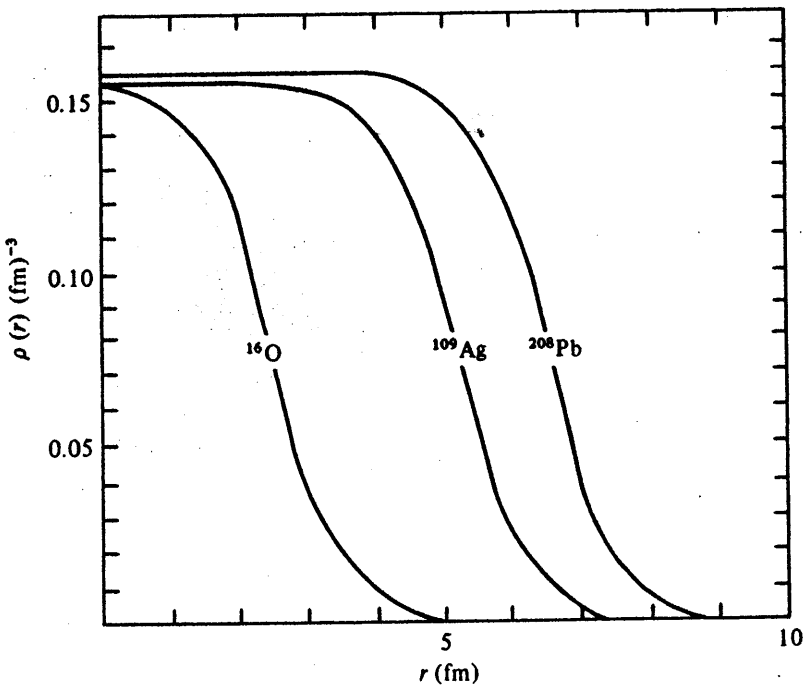

Fig. 4.4 The nucleon density of the nuclei of Fig. 4.3, with $\rho(r) = (A/Z)\rho_{ch}(r)$.

Figure 14-8
Parametrization of the nuclear charge density.

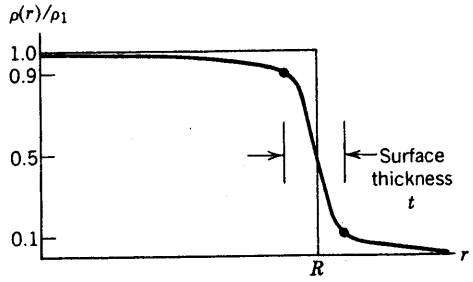

formula

$$R = R_0 A^{1/3} \tag{14-3}$$

and produces constant parameters with the approximate values

$$t = 2.4 \text{ fm} \quad \text{and} \quad R_0 = 1.07 \text{ fm}$$

over the whole survey of nuclei. Other methods of determining the nuclear radius confirm the A dependence of Equation (14-3). In general, these techniques employ the parameter R_0 alone and yield values of R_0 in the range 1.18–1.40 fm.

The decrease of the central charge density $\rho(0)$ is a noteworthy feature of Figure 14-9. This behavior opposes the tendency for neutrons to outnumber protons with

Figure 14-9
Nuclear charge densities deduced from electron scattering. The cases illustrated correspond to the nuclei considered in Figure 14-7.

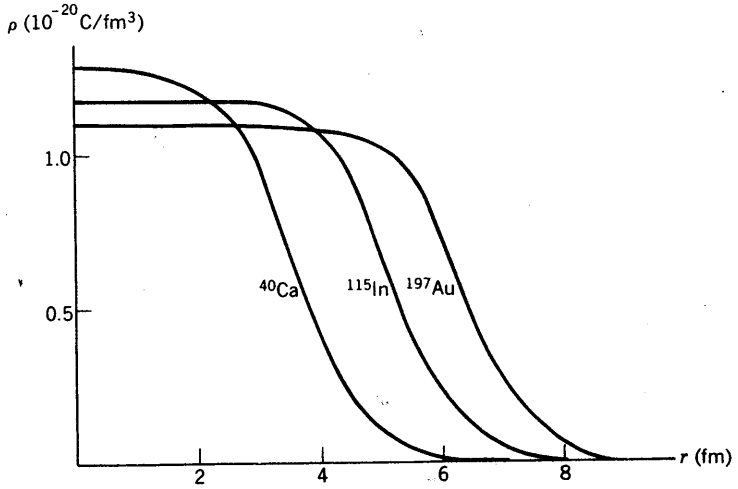

which implies

$$R = 1.12\, A^{\frac{1}{3}} \text{ fm}.$$

4.4 The masses and binding energies of nuclei in their ground states

It thus appears that a nucleus is rather like a spherical drop of liquid, of nearly uniform density. How are we to understand its properties? A nucleus is a quantum-mechanical system. We shall see later that its excited states are generally separated by energies ~ 1 keV or more from its ground state, so that to all intents and purposes nuclei in matter at temperatures that are accessible on Earth are in their ground states. Like any other finite system, a nucleus in its ground state has a well-defined energy and a well-defined angular momentum. In this chapter we shall be concerned with the ground-state energy. Other ground-state properties of a nucleus will be discussed in the next chapter.

Since a nucleus is a bound system, an energy $B(Z, N)$ is needed to pull it completely apart into its Z protons and N neutrons. From the Einstein relation between mass and energy, the *binding energy* $B(Z, N)$ is related to the mass $m_{\text{nuc}}(Z, N)$ of the nucleus by

$$m_{\text{nuc}}(Z, N) = Zm_{\text{p}} + Nm_{\text{n}} - B(Z, N)/c^2, \tag{4.3}$$

and $B(Z, N)$ must be positive for the nucleus to be formed. We shall see that nuclear binding energies are of the order of 1% of the rest-mass energy $m_{\text{nuc}}c^2$.

Experimentally, the masses of atomic ions, rather than the masses of bare nuclei, are the quantities usually measured directly. If $m_a(Z, N)$ is the mass of the neutral atom,

$$m_a(Z, N) = Z(m_{\text{p}} + m_{\text{e}}) + Nm_{\text{n}} - B(Z, N)/c^2 - b_{\text{electronic}}/c^2, \tag{4.4}$$

where $b_{\text{electronic}}$ is the binding energy of the atomic electrons. These electronic contributions are, for many purposes, negligible. (The simple Thomas–Fermi statistical model of a neutral atom gives the total electronic binding energy $\approx 20.8Z^{\frac{7}{3}}$ eV.)

Atomic masses are known very accurately, and published tables give atomic masses rather than nuclear masses. Measurements in 'mass spec-